Original article
DOI: https://doi.org/10.18721/JPM.15304

EXPERIENCE OF USING SEMIEMPIRICAL DIFFERENTIAL MODELS OF TURBULENCE FOR CALCULATION OF LIQUID-METAL CONVECTION IN A BOTTOM HEATED CYLINDER

S. I. Smirnov✉, *E. M. Smirnov*

Peter the Great St. Petersburg Polytechnic University, St. Petersburg, Russian Federation

✉ sergeysmirnov92@mail.ru

Abstract. The paper deals with assessments of ability of the three RANS turbulence models (k-ω SST, k-ε RNG and one of the differential RSM formulations) to predict local and integral characteristics of the statistically 3D Rayleigh – Bénard liquid-metal convection with a key role of large-scale circulation (LSC). URANS-based calculations at the Rayleigh number of 10^6 and the Prandtl number of 0.025 have been performed for a bottom heated cylindrical container with equal diameter to height, using computational grids of varied cell sizes. The case of the slightly tilted container was considered where the LSC azimuth position being fixed. The suitability of the used turbulence models was evaluated by comparing the obtained results with the direct numerical simulation data obtained earlier for the same conditions.

Keywords: Rayleigh – Bénard convection, large scale circulation, RANS model, turbulence, cylinder

Funding: The research has been funded in part by the Ministry of Science and Higher Education of the Russian Federation, within the framework of strategic academic leadership "Priority 2030" (Agreement No. 075-15-2021-1333 dated September 30, 2021)

C**itation:** Smirnov S. I., Smirnov E. M., Experience of using semiempirical differential models of turbulence for calculation of liquid-metal convection in a bottom heated cylinder, St. Petersburg Polytechnical State University Journal. Physics and Mathematics. 15 (3) (2022) 43–60. DOI: https://doi.org/10.18721/JPM.15304

Научная статья
УДК 536.25
DOI: https://doi.org/10.18721/JPM.15304

ОПЫТ ПРИМЕНЕНИЯ ПОЛУЭМПИРИЧЕСКИХ ДИФФЕРЕНЦИАЛЬНЫХ МОДЕЛЕЙ ТУРБУЛЕНТНОСТИ ДЛЯ РАСЧЕТА КОНВЕКЦИИ ЖИДКОГО МЕТАЛЛА В ПОДОГРЕВАЕМОМ СНИЗУ ЦИЛИНДРЕ

С. И. Смирнов✉, *Е. М. Смирнов*

Санкт-Петербургский политехнический университет Петра Великого,

Санкт-Петербург, Россия

✉ sergeysmirnov92@mail.ru

Аннотация. Статья содержит оценку возможностей трех известных RANS-моделей турбулентности (k-ω SST, k-ε RNG и одной из дифференциальных RSM-моделей) по предсказанию локальных и интегральных характеристик статистически трехмерной рэлей-бенаровской конвекции жидкого металла с определяющей ролью крупномасштабной циркуляции (КМЦ). Расчеты на основе Unsteady-RANS-подхода на различных по измельченности сетках проведены при числе Рэлея 10^6 и числе Прандтля 0,025 для подогреваемой снизу цилиндрической емкости при равенстве ее диаметра высоте. Рассмотрен случай слабого наклона объекта, когда в нем КМЦ принимает «зафиксированное» азимутальное положение. Работоспособность использованных моделей турбулентности оценивается через сопоставление результатов с ранее полученными данными прямого численного моделирования для тех же условий.

Ключевые слова: конвекция Рэлея – Бенара, крупномасштабная циркуляция, турбулентность, осредненные по Рейнольдсу уравнения

Финансирование: Исследование частично финансировалось Министерством науки и высшего образования Российской Федерации в рамках программы стратегического академического лидерства «Приоритет 2030» (Соглашение 075-15-2021-1333 от 30.09.2021).

Ссылка для цитирования: Смирнов С. И., Смирнов Е. М. Опыт применения полуэмпирических дифференциальных моделей турбулентности для расчета конвекции жидкого металла в подогреваемом снизу цилиндре // Научно-технические ведомости СПбГПУ. Физико-математические науки. 2022. Т. 15. № 3. С. 43–60. DOI: https://doi.org/10.18721/JPM.15304

Introduction

A characteristic feature of free convective flow developing in cylindrical containers heated from below is the presence of large-scale vortex structures occupying the entire domain (see, for example, reviews [1, 2]). In particular, if the diameter of the cylinder is equal to its height, the predominant structure of convective flow is a single vortex, also called a convection cell, or large-scale circulation (LSC) [3–7]. LSC in a strictly vertically oriented container with axially symmetric boundary conditions does not have a dedicated azimuthal position and, accordingly, nothing prevents it from occasionally making random movements in the azimuthal direction. This is confirmed by both experimental [8–11] and numerical [12–15] studies of turbulent Rayleigh–Bénard convection in cylindrical containers. The specific azimuthal behavior of LSC is determined in experimental studies by small deviations from axial symmetry that are difficult

to control, inevitably present in laboratory models. The azimuthal instability of a convection cell is also generally manifested in numerical studies, where the 'external' factor affecting the random oscillations of LSC is the asymmetry of the computational grid or the peculiarities of numerical algorithms.

The random azimuthal movements of the convection cell make it incredibly difficult to obtain statistical data on its three-dimensional structure, including the quantities characterizing the 'background' turbulence: fields of Reynolds stresses and turbulent heat flux. However, these low-frequency movements can be suppressed, thus 'locking' the LSC in a certain azimuthal position if a stabilizing external factor is artificially introduced; this can be achieved, for example, by slightly tilting the container. This method for 'locking' the LSC is used in experimental [8, 16–20] and numerical [20–24] studies.

The Direct Numerical Simulation (DNS) method is widely used to describe turbulent Rayleigh-Bénard convection in regions with relatively simple geometry. This approach assumes that all scales of turbulent fluid flow are resolved, consequently proving to be the most informative (see, for example, [25–30] for the case of a vertically oriented cylinder and [23, 24] for the case of a slightly tilted container). However, large computational costs are required for resolving the entire spectrum, increasing very quickly with increasing Rayleigh numbers.

The Large Eddy Simulation (LES) method allows reducing the costs, in particular, in its 'simplified' version, the Implicit LES (ILES), where subgrid-scale turbulent viscosity is not introduced explicitly into the transport equations, and the dissipative properties of the numerical scheme play the role of physical viscosity on a small scale. The experience of adopting the ILES approach for modeling the turbulent Rayleigh–Bénard convection in cylindrical containers is described in [22, 31, 32]. A recent paper [33] applied the ILES method to studying anisotropy of turbulent transfer in mixed convective flow developing in the crucible of a Czochralski furnace for growing silicon crystals.

It is well known, however, that as the Rayleigh number increases, computations of convective flow by the LES method require progressively refining the grids in the near-wall layers, with the refinements introduced in all spatial directions. As a result, obtaining reliable numerical data for a wide range of practical problems characterized by high Rayleigh numbers also involves very high computational costs.

In view of this, strong interest persists in numerical modeling of turbulent free and mixed-convection flows based on Reynolds-averaged Navier–Stokes (RANS) equations, closed by some semi-empirical differential model of turbulence. It should be borne in mind, however, that the options for obtaining a steady RANS solution are very limited in the case of Rayleigh–Bénard convection, depending on the turbulence model applied. It is therefore worthwhile to explore a problem statement developed to incorporate computations based on unsteady Reynolds equations. This approach is interpreted as Unsteady RANS (URANS) or Transient RANS (TRANS).

Refs. [34–36] thoroughly analyze the applications of the URANS approach to reproducing unsteady coherent structures and the intensity of turbulent transfer in the 'classical' statistically one-dimensional case of free convection between two differently heated horizontal plates. The authors emphasize the presence of two different scales in the motion: large amplitudes associated with plumes, thermals and convection cells, as well as turbulence arising mainly in the near-wall boundary layers and carried by large-scale structures. This makes turbulent Rayleigh–Bénard convection very convenient for computations based on unsteady Reynolds equations. The computational results [34–36] obtained by the URANS method closed by a three-parameter turbulence model indicate that the averaged temperature profile, second-order moments and integral heat transfer are in good agreement with the data of most DNS calculations and experimental data on convection between horizontal plates.

Recent years saw growing interest towards RANS simulations of free convective flows, closed by some model from the RSM family (Reynolds Stress Model) based on either steady or unsteady statements [37–41]. In general, the RSM model solves differential equations for transport of all components of the Reynolds stress tensor and the turbulent heat flux vector. Efforts to somewhat simplify the model, lowering the computational costs, are concentrated on 'reduced' formulations where differential transport equations are solved only for Reynolds stresses, and the turbulent heat flux is computed based on the gradient hypothesis in terms of averaged flow parameters.

The experience of using Reynolds stress models to computing turbulent free-convection flows in the gravitational field presented in the literature mainly covers model configurations with differently heated vertical walls or the case of a boundary layer near a vertical heated surface [37–41].

This paper adopts one of the well-known RSM models (implemented, in particular, in the ANSYS Fluent software package) for URANS simulations of mercury convection in a slightly tilted cylinder heated from below. Similar simulations are also carried out for two turbulence models with isotropic viscosity from the k-ω and k-ε families. The computed statistical characteristics of the first and second orders are compared with the data in [23] obtained earlier for the given configuration based on the DNS approach.

Problem statement and mathematical model

We consider turbulent convection of fluid in a bottom-heated cylindrical container with a single aspect ratio ($\Gamma = D/H = 1$). The container is tilted by a small angle ($\varphi = 2°$) with respect to the gravity vector **g** (Fig. 1,*a*).

No-flow and no-slip conditions are imposed on all boundaries of the container. Horizontal walls are assumed to be isothermal: the temperature T_h of the top wall is higher than that of the bottom wall (T_c). The side wall is treated as adiabatic.

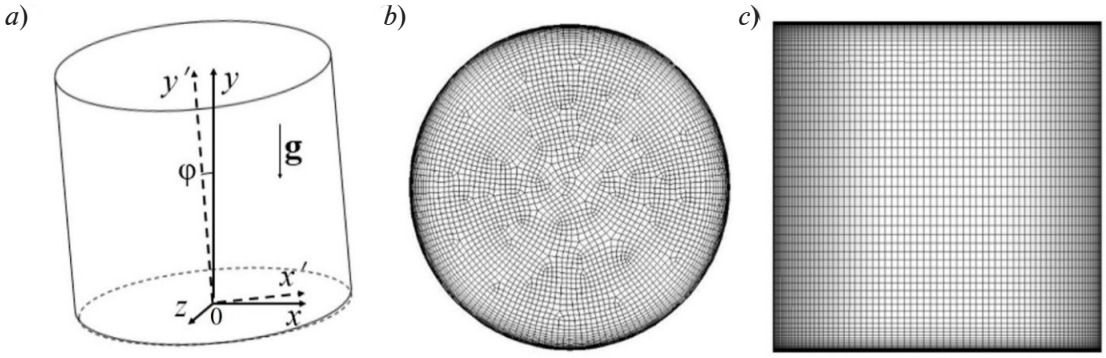

Fig. 1. Images of cylindrical container for the problem statement: *a* corresponds to the geometry of the computational domain; *b*, *c* show characteristic views of the computational grids in horizontal (*b*) and central vertical (*c*) planes

The dimensionless governing parameters of the problem were the Prandtl number $\mathrm{Pr} = \mu C_p/\lambda$ and the Rayleigh number

$$\mathrm{Ra} = \mathrm{Pr}\cdot(\rho^2 g\beta\Delta T H^3/\mu^2),$$

where μ is the dynamic viscosity; C_p is the specific heat at constant pressure; λ is the thermal conductivity; ρ is the density; β is the volumetric expansion coefficient; g is the gravity acceleration; ΔT is the temperature difference between the hot and cold walls, $\Delta T = T_h - T_c$.

The characteristic (large-scale) velocity of the flow (buoyant velocity) is the quantity $V_b = (g\beta\Delta T H)^{0.5}$. The time scale is the characteristic convective time $t_b = H/V_b$.

The computations presented were carried out for the values of hydrodynamic numbers $\mathrm{Pr} = 0.025$ and $\mathrm{Ra} = 10^6$.

Convective motion is calculated from a system of unsteady Reynolds-averaged equations of dynamics and heat transfer (1)–(3), which includes the Navier–Stokes equations written in the Bussinesq approximation to account for buoyancy effects in the gravitational field, the continuity equation and the energy equation:

$$\frac{\partial V_j}{\partial x_j} = 0, \tag{1}$$

$$\rho\frac{\partial V_i}{\partial t} + \rho V_j\frac{\partial V_i}{\partial x_j} = -\frac{\partial p}{\partial x_i} + \frac{\partial\left(\tau_{ij} + \tau_{t,ij}\right)}{\partial x_j} - \rho\beta\left(T - T_0\right)g_i, \tag{2}$$

$$\rho C_p \frac{\partial T}{\partial t} + \rho C_p V_j \frac{\partial T}{\partial x_j} = \frac{\partial}{\partial x_j}\left(q_j + q_{t,j}\right). \quad (3)$$

The equations are solved in the coordinate system associated with the cylindrical container $x_j = (x', y', z' = z)$ shown in Fig. 1,*a*. The notations V_i and T correspond to the components of Reynolds-averaged velocity ($i(j) = 1, 2, 3$) and temperature; τ_{ij}, q_j are the components of the viscous stress tensor and the diffusive heat flux calculated in terms of the Reynolds-averaged values:

$$\tau_{ij} = \mu\left(\frac{\partial V_i}{\partial x_j} + \frac{\partial V_j}{\partial x_i}\right), \quad (4)$$

$$q_j = -\lambda \frac{\partial T}{\partial x_j}. \quad (5)$$

The quantities $\tau_{t,ij}$, $q_{t,j}$ entering Eqs. (2), (3) are the components of the turbulent (Reynolds) stress tensor and the turbulent heat flux vector arising from Reynolds averaging and reflecting the presence of relatively high-frequency fluctuations of velocity v_i and the temperature θ in the instantaneous motion.

Respectively,

$$\tau_{t,ij} = -\rho\overline{v_i v_j}, \quad (6)$$

$$q_{t,j} = -\rho C_p \overline{v_j \theta}, \quad (7)$$

where the overbar indicates Reynolds averaging.

The system of equations (1)–(3) is not closed. To close the system, we should determine the method (model) for calculating the quantities $\tau_{t,ij}$ and $q_{t,j}$.

The calculated data presented in this paper are obtained when the system (1)–(3) is closed with respect to three models.

The *k*-ε RNG and *k*-ω SST models. These models belong to the class of two-parameter differential turbulence models based on the concept of isotropic turbulent viscosity (the Bussinesq hypothesis). According to this concept, the components of the turbulent stress tensor and the turbulent heat flux vector are related to the Reynolds-averaged flow parameters as follows:

$$\tau_{t,ij} = \mu_t\left(\frac{\partial V_i}{\partial x_j} + \frac{\partial V_j}{\partial x_i}\right) - \frac{2}{3}k\delta_{ij}, \quad (8)$$

$$q_{t,j} = -\lambda_t \frac{\partial T}{\partial x_j}, \quad (9)$$

where μ_t is the turbulent viscosity determined from the calculated turbulence parameters (k, ε or ω); λ_t is the turbulent thermal conductivity, $\lambda_t = C_p\mu_t/\mathrm{Pr}_t$ (Pr_t is the turbulent Prandtl number (taken equal to 0.8 in this calculation)); k is the turbulent kinetic energy.

The complete formulation for the *k*-ε RNG and *k*-ω SST models is given in [42] and [43, 44], respectively.

Reynolds stress model. The differential model of Reynolds stresses implemented in the ANSYS Fluent 18.2 package was used in this study. Transport equations are only solved for turbulent stresses within the model, while the components of turbulent heat flux are calculated in terms of the averaged flow parameters based on the gradient hypothesis.

The transport equations for Reynolds stresses equations are generally formulated as follows:

$$\rho\frac{\partial\left(\overline{v_i v_j}\right)}{\partial t}+\rho V_j\frac{\partial\left(\overline{v_i v_j}\right)}{\partial x_j}=D_{ij}^m+D_{ij}^t+R_{ij}+G_{ij}+\varphi_{ij}-\varepsilon_{ij}, \tag{10}$$

where D_{ij}^m, D_{ij}^t are the terms reflecting molecular (m) and turbulent (t) diffusive transport; R_{ij}, G_{ij} are the terms characterizing the kinetic energy generated by averaged motion and by buoyancy forces, respectively; φ_{ij} is the quantity responsible for the redistribution of energy between stress and strain velocity tensors; ε_{ij} is the dissipative term.

A differential equation for transport of the quantity ω (the specific dissipation rate of kinetic energy used to close Eq. (10)) is solved together with the equations for the Reynolds stresses. The Stress Omega option was selected during the computations from the options available in the ANSYS Fluent package and defining the specific form of this equation.

The components of turbulent heat flux $\overline{v_i\theta}$ are calculated by the formulas:

$$\overline{v_i\theta}=\frac{\mu_t}{\rho\,\mathrm{Pr}_t}\frac{\partial T}{\partial x_i},\ \mu_t=\frac{\rho k}{\omega},\ k=\frac{1}{2}\overline{v_i v_i}, \tag{11}$$

where $\mathrm{Pr}_t = 0.8$ (the same as above).

The components of the Reynolds stress model are described in [45–47], as well as in the user documentation for the ANSYS Fluent 18.2 software package.

Specifics of computations and data processing

Comparative computations based on the ANSYS Fluent finite volume method were carried out on two grids consisting of hexagonal elements containing 0.47 million (C1 grid) and 3.7 million cells (C2 grid). The structure of the grids in transverse and longitudinal (central) planes is illustrated in Fig. 1, *b*, *c*. The grids were clustered to the walls, while the size of the near-wall element was $1.5\cdot10^{-4}$ N. A characteristic feature of the grids was the presence of a central 'unstructured' (asymmetric) subdomain about $0.8D$ in diameter (see Fig. 1, *b*).

Preliminary computations led us to conclude that none of the turbulence models applied is capable of providing a steady-state solution to the problem. All subsequent computations were performed in an unsteady formulation. The non-iterative fractional step method with second-order accuracy was applied to advance in physical time. The time step was about one hundredth of the large-scale time t_b of the problem, which was about 10 times higher than that used in [23] for computations by the DNS method.

The spatial approximation of convective terms in the transport equations was carried out by the QUICK scheme with nominally third-order accuracy. Diffusion terms were approximated by a central-difference scheme with second-order accuracy.

All computations started from a zero initial velocity field and uniform temperature field taken as $(T_c + T_h)/2$. Samples for the time averaging performed after a transition region were equal to $3000t_b$ in all computations.

The computational data were processed to obtain the first-order and second-order statistical characteristics based on the following assumptions.

First, it was assumed that the instantaneous velocities and temperatures present in the real current (marked with an asterisk) can be decomposed into low- and high-frequency components:

$$V_i^*=V_i+v_i,\ T^*=T+\theta. \tag{12}$$

Secondly, it was assumed that Reynolds-averaged motion contains only low-frequency 'large-scale' components of velocity and temperature fields, i.e.,

$$\overline{V_i^*}=V_i,\ \overline{T^*}=T, \tag{13}$$

which, in turn, can be decomposed into mean values t_{avr} obtained by averaging over a sufficiently large time sample and fluctuation components:

$$V_i = \langle V_i \rangle + V_i', \; T = \langle T \rangle + T'. \tag{14}$$

The angle brackets ⟨…⟩ here indicate time averaging, and the prime indicates the fluctuations. In this case,

$$\langle V_i^* \rangle = \langle V_i \rangle, \langle T^* \rangle = \langle T \rangle. \tag{15}$$

Let us introduce further notations for second-order statistical characteristics (second moments):

$$P_{ij}^t = \langle V_i^* V_j^* \rangle - \langle V_i^* \rangle \langle V_j^* \rangle, \tag{16}$$

$$Q_i^t = \langle V_i^* T^* \rangle - \langle V_i^* \rangle \langle T^* \rangle, \tag{17}$$

which are the components of the total turbulent stress tensor (taken with the reverse sign) and the total heat flux vector.

Taking into account the decompositions (12), (14), we obtain:

$$P_{ij}^t = \langle V_i' V_j' \rangle + \langle \overline{v_i v_j} \rangle + \langle V_i' v_j \rangle + \langle v_i V_j' \rangle, \tag{18}$$

$$Q_i^t = \langle V_i' T' \rangle + \langle \overline{v_i \theta} \rangle + \langle V_i' \theta \rangle + \langle v_i T' \rangle. \tag{19}$$

The first terms in the right-hand sides of expressions (18) and (19) reflect the contribution from numerically resolved components of the motion, the second ones reflect the contribution from simulated components, the third and fourth ones are the so-called cross terms which we are forced to discard (as it was done in [34–36]), due to the assumption of weak correlation between the low- and high-frequency components of motion. It is generally estimated *a posteriori* whether such an assumption is acceptable for a continuous fluctuation spectrum in instantaneous turbulent flow, that is, by comparison with 'reference' data of numerical and experimental studies.

Thus, for comparison with the data from [23], obtained earlier by the DNS method, the values of total turbulent stresses, the components of the total turbulent heat flux and the total kinetic energy of oscillatory motion were calculated as

$$P_{ij}^t = \langle V_i' V_j' \rangle + \langle \overline{v_i v_j} \rangle, \tag{20}$$

$$Q_i^t = \langle V_i' T' \rangle + \langle \overline{v_i \theta} \rangle, \tag{21}$$

$$K^t = \frac{1}{2} P_{ii}^t. \tag{22}$$

The computations by the Reynolds stress model determined the contribution from the simulated component of P_{ij}^t by averaging the Reynolds stresses obtained during the time t_{avr} by solving transport equations (10).

The contribution of the simulated component to the total turbulent heat flux was estimated as follows:

$$\langle \overline{v_i \theta} \rangle = \left\langle \frac{\mu_t}{\rho \, \mathrm{Pr}_t} \frac{\partial T}{\partial x_i} \right\rangle \approx \frac{\langle \mu_t \rangle}{\rho \, \mathrm{Pr}_t} \frac{\partial \langle T \rangle}{\partial x_i}. \tag{23}$$

This expression is obtained based on the gradient hypothesis (11) assuming a weak correlation between the fluctuations of turbulent viscosity and numerically resolved fluctuations of temperature.

Computational results and discussion

The computational results are given below in dimensionless form. The coordinate values are taken relative to container height H. This implies the following correspondence:

$$x_{i(j)} = x', y', z' \text{ for } i(j) = 1, 2, 3.$$

The velocity components are taken relative to the buoyant velocity V_b, the turbulent stresses P_{ij}^t and kinetic energy K^t to the square of buoyant velocity; the components of turbulent heat flux Q_i^t are normalized by the product $V_b \Delta T$.

Time-averaged flow fields and local heat transfer. Fig. 2, *a* illustrates an averaged picture of mercury convection in a bottom-heated cylinder with pronounced LSC predicted from URANS computations for different turbulence models.

Fig. 2,*b* shows the field of time-averaged axial velocity component $\langle V_{y'} \rangle$ in the central vertical plane of the cylinder. Evidently, when LSC is 'locked' in this azimuthal position, the flow is symmetrical relative to the plane $x'0y'$. Distributions of the averaged axial velocity along the coordinate x' in the same plane (Fig. 2,*c*), computed for different RANS-models, are almost identical and very close to the distribution obtained in our previous study [23] by the DNS method.

The mean temperature distributions along the central container axis, computed for the three RANS models, are compared with each other and with the DNS data in Fig. 2,*d*. There is generally good agreement between the results obtained by different models/approaches: in particular, all of them predict an extended central zone with an inverse temperature gradient. On the other hand, more detailed analysis of the distributions in the area adjacent to the end wall (see the enlarged fragment in Fig. 2,*d*) allows us to conclude that in the case of the k-ε RNG model, the temperature gradient in this area, and therefore the local heat flux on the wall, is somewhat lower (by 2–3%) than in the case of the other two RNS models, which predict gradient values that virtually coincide with the result of the DNS computations.

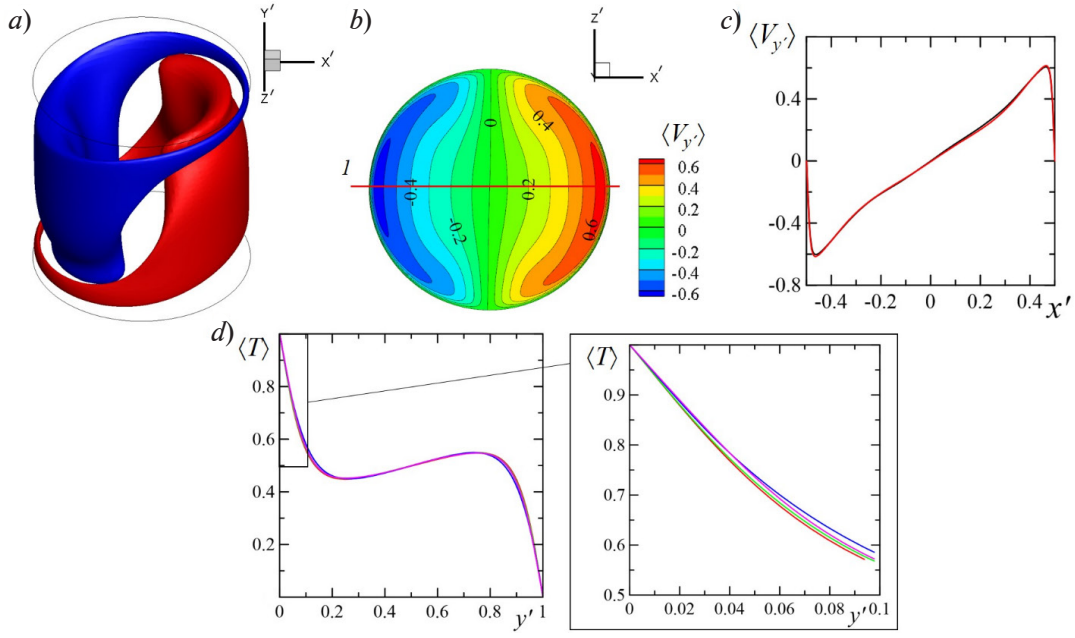

Fig. 2. Comparison of the curves for the computed quantities of the problem, obtained using different models: URANS (*a, b*), URANS, DNS (*c*), DNS, RSM, k-ω SST, k-ε RNG (*d*).

The figure shows isosurfaces of time-averaged axial velocity component of upward (red) and downward (blue) flow, $|\langle V_y \rangle| = 0.3$ (*a*); the field of averaged axial velocity component in the central plane (*b*), as well as the distribution of this velocity along line *1* (the two curves coincide) (*c*); the distribution of averaged temperature along the container axis by the DNS (red curves), RSM (green), k-ω SST (blue), k-ε RNG (lilac) (*d*) models

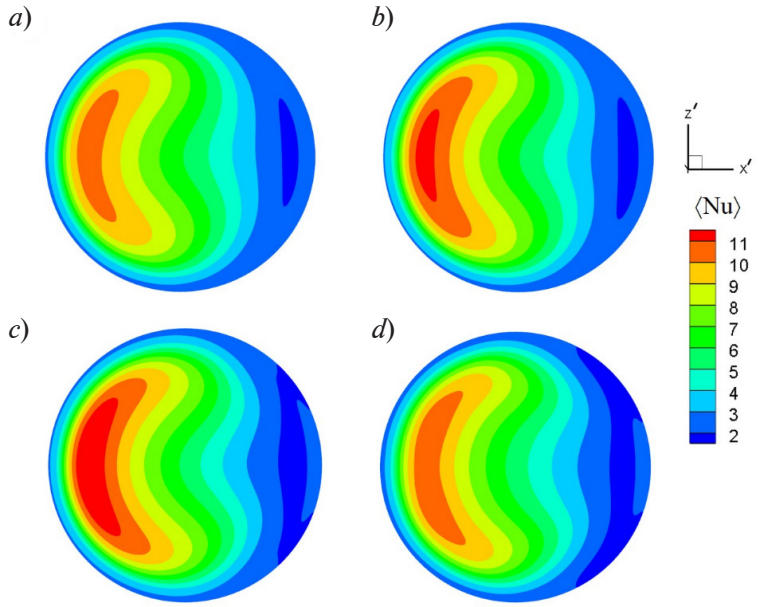

Fig. 3. Distributions of the time-averaged local Nusselt number on the lower cylinder wall, obtained using different models: DNS [23] (*a*), RSM (*b*), *k*-ω SST (*c*) and *k*-ε RNG (*d*)

Fig. 3 shows the distributions of the time-averaged local Nusselt number on the lower wall, illustrating, in particular, strong spatial non-uniformity of this quantity due to the presence of LSC. The results of RANS computations show very satisfactory agreement with the DNS data, especially for the RSM model: in this case, not only a crescent-shaped zone of maximum heat transfer is reproduced, but also a well-defined region of the lowest values of the Nusselt number.

Averaging of the distributions shown in Fig. 3 over the wall surface yields the integral Nusselt numbers given in the table. Apparently, these values obtained by different RNS models differ from the DNS data by no more than 3.6%; a deviation towards lower values is observed for the *k*-ε RNG model, and towards higher values for the other two models. The Reynolds stress model gives the result closest to the one obtained by the DNS method.

Concluding this subsection, we should note that the URANS computations presented in it were obtained using the C1 grid. Similar computations were performed on a C2 grid which contained more cells (almost by an order of magnitude). Time-averaged distributions/profiles of velocity, temperature and local Nusselt number computed on two grids were found to be virtually the same (up to the thickness of the visualized curves). The integral Nusselt numbers differed only in the fourth digit. Thus, we can conclude for a related family of problems on three-dimensional Rayleigh-Bénard convection of liquid metal that the grid size of about half a million cells is sufficient to predict first-order statistical data based on the URANS approach at Rayleigh numbers of the order of 10^6.

Table

Comparison of integral Nusselt numbers, obtained from different RANS models, with DNS data

Model	*k*-ε RNG	*k*-ω SST	RSM	DNS [23]
Nu	5.46	5.84	5.78	5.64

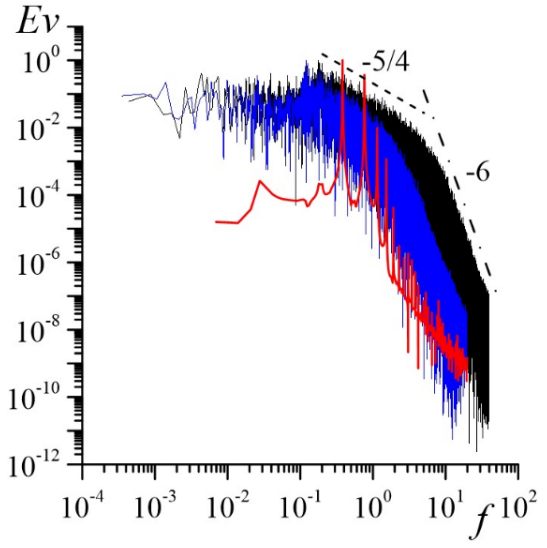

Fig. 4. Energy spectra for fluctuations of the axial velocity component $V_{y'}$ at the point located at $x' = 0.35$ at the intersection of the plane $x'0y'$ and the central vertical plane (see Fig. 1, *a*); the data were obtained from different models: DNS [23] (black curve), RSM (blue curve), k-ε RNG (red curve); approximations by the functions $Ev \sim f^{-5/4}$ (dashed line) and f^{-6} (dot-dashed line)

Spectral characteristics. Fig. 4 shows the energy spectra for the fluctuations of the axial velocity component at a point located at $x' = 0.35$ at the intersection of the $x'0y'$ plane and the central vertical plane. The spectra obtained in computations on a refined grid (C2, 3.7 million cells) for the RSM and k-ε RNG models are compared with the spectrum from [23], computed by the DNS method on a grid containing about 15 million cells. Notice that the spectrum calculated by the k-ω SST model practically coincides with the spectrum obtained using the Reynolds stress model (not shown in Fig. 4).

The spectrum obtained for the RSM model (as well as for k-ω SST) indicates that turbulent fluctuations are numerically resolved in a noticeable part of the quasi-inertial ramge, more pronounced in the case of DNS computations and suggesting a decrease in the spectral density proportionally to $f^{-5/4}$; this decrease rate is close to the classical law $Ev \sim f^{-5/3}$ (Ev is the spectral energy density, non-dimensionalized by its maximum value, f is the dimensionless frequency) for the inertial range in the case of developed isotropic turbulence. Accordingly, the transition to a pronounced 'dissipative' region characterized by rapid decrease, approximately proportional to f^{-6}, occurs earlier compared to DNS. Conversely, the k-ε RNG model predicts unsteady convection with quasi-periodic oscillations covering the region of intermediate frequencies. The difference in the results obtained by the k-ω SST and k-ε RNG models is primarily due to the fact that the latter generates a significantly higher level of turbulent viscosity compared to the k-ω SST model.

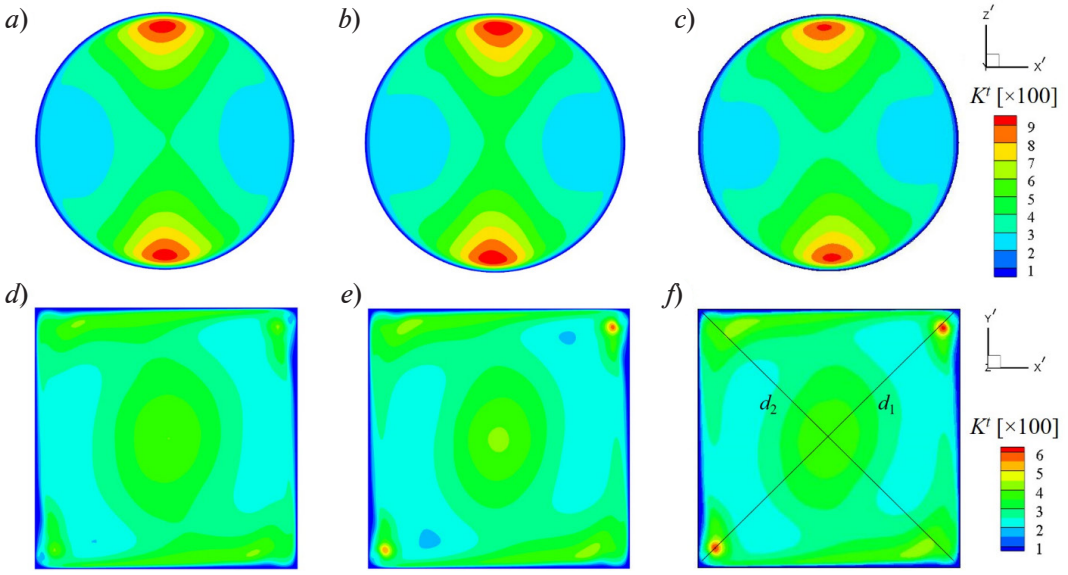

Fig. 5. Distributions of turbulent kinetic energy in two central planes of the cylinder obtained by RSM (*a*, *b*, *d*, *e*) and DNS [23] (*c*, *f*) models, as well as using C1 (*a*, *d*) and C2 (*b*, *e*) grids

Turbulent stresses and turbulent heat flux. Next, we consider the results obtained by the RANS models for second-order moments.

Fig. 5 illustrates the effect that the dimension of the computational grid has on the predictive capability of the RSM model for the characteristic features observed in the field of turbulent kinetic energy, compared with the DNS data.

These features are as follows:

1) the most intense level of fluctuations (red and yellow zones in Fig. 5, *a*–*c*) is observed in the mixing layers formed upon interaction of upward and downward flows in LSC;

2) extremely weak oscillatory motion is observed in the zones of strong upward and downward flows, while kinetic energy takes minimum values in these areas;

3) small zones with elevated kinetic energies are observed in the corners (red and yellow 'spots' in Fig. 5, *e*, *f*), where the corner vortices formed are, on average, stationary (this was established in [23]) and, accordingly, the mixing layers with a global vortex in the form of LSC. The first two features are well reproduced in the computations by the RSM model on both grids, while the third one cannot be predicted using a coarse grid (see Fig. 5,*d*). The same applies to the turbulent stress fields in the corners, which are analyzed below.

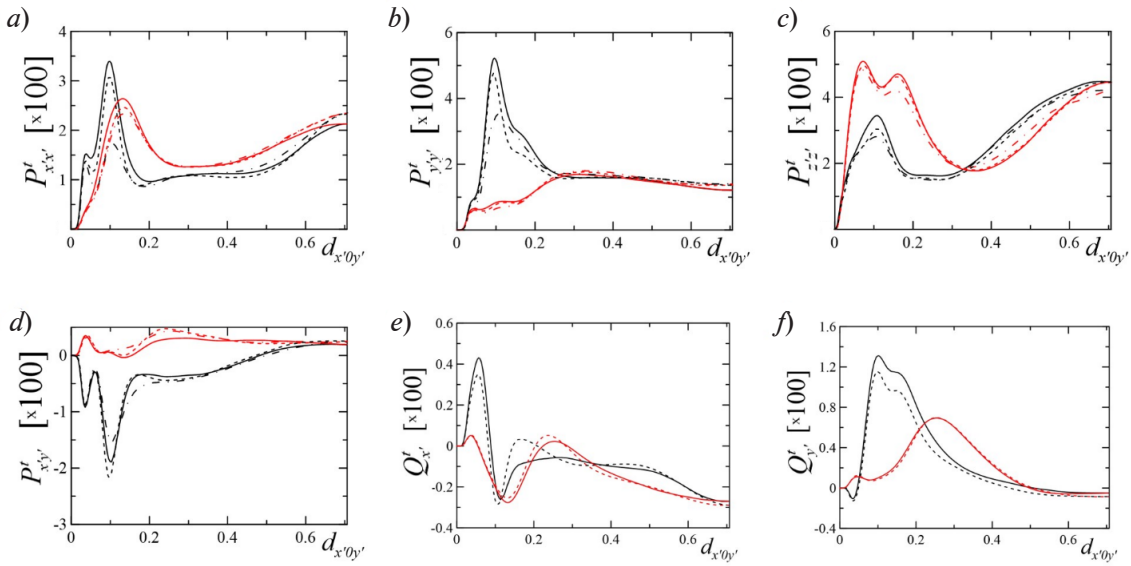

Fig. 6. Component distributions for turbulent stress tensor (*a*–*d*) and turbulent heat flux vector (*e*, *f*) along the diagonals d_1 (black curves) and d_2 (red curves) (see Fig. 5, *f*). Data were obtained from different models: DNS [23] (solid curves), URANS simulations by the RSM model (remaining curves), C1 (dash-dots) and C2 (dashes) grids

Fig. 6 shows the computational distributions for the distributions of the total turbulent stress tensor and the turbulent heat flux vector along the diagonals of the central longitudinal section of the container (see Fig. 5,*f*). The analysis of factors determining the form of the curves presented is carried out in our earlier study [23]. The curves for URANS computations by the RSM model reflect the total contribution from two components of the values considered: numerically resolvable and simulated. It can be seen that the results of URANS computations on the C2 grid are in very good agreement with the DNS data. As noted above, the coarse C1 grid does not reproduce the features of second-order statistics in the mixing layers formed by the interaction of corner vortices and LSC: this drawback is clearly traced from the computational results in Fig. 6, *a*, *b*. In view of this, the results of URANS computations of the turbulent heat flux vector (see Fig. 6, *e*, *f*) are shown only for the refined grid. Generally good agreement with the DNS data is also observed here.

Fig. 7 compares the axial component profiles of turbulent heat flux, obtained from different turbulence models for the line coinciding with the cylinder axis, with the DNS data; contributions from numerically resolved and simulated components of the flux, as well as their total contribution are given in the figure. Pronounced differences can be observed between the computational

results from different RANS models. The Reynolds stress model gives comparable values for both components of the total flux for the region $|y_r| < 0.2$ with large mean temperature gradients (see Fig. 2, *d*); however, the resolved component is clearly predominant.

Conversely, the simulated component is predominant for the case of the *k*-ω SST model (Fig. 7, *b*), while the contribution of the resolved component is practically absent for the *k*-ε RNG model. The latter circumstance is obviously due to an elevated level of turbulent viscosity in the case of the *k*-ε RNG model and the relatively low intensity of the predicted quasi-periodic flow. Accordingly, the *k*-ε RNG model gives the worst predictions for the profile of the total turbulent heat flux.

As evident from Fig. 7, the results obtained from the Reynolds stress model are in excellent agreement with the DNS data, even though a simplified approach adopting the gradient hypothesis was used to estimate the simulated component. Therefore, we can conclude that there is no need to solve differential equations for transport of turbulent heat flux components in the case of URANS simulations of Rayleigh–Bénard convection with three-dimensional LSC, carried out by the Reynolds stress model on sufficiently refined grids.

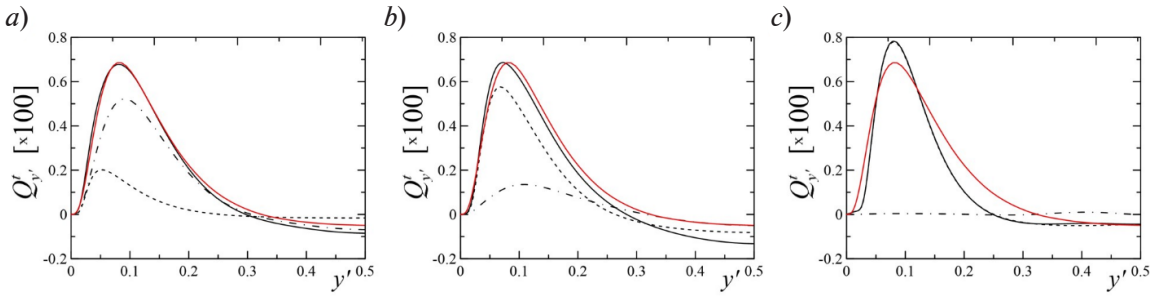

Fig. 7. Distributions for axial component of turbulent heat flux along the cylinder axis; comparison between the computational data from different RANS-models (black curves) and DNS data [23] (red curves), as well as between the contributions from components of turbulent heat flux: simulated (dashes), numerically resolved (dot-dashes) and the total of two components (solid lines). RANS models: RSM (*a*), *k*-ω SST (*b*), *k*-ε RNG (*c*)

Conclusion

The paper assesses the predictive capabilities of three different turbulence RANS models (*k*-ω SST, *k*-ε RNG and one of the well-known differential RSM-models) for local and integral characteristics of statistically three-dimensional Rayleigh–Bénard convection of liquid metal with the decisive role played by large-scale circulation (LSC). The conclusions are based on the computational results for unsteady convection (Unsteady RANS) in a slightly tilted cylindrical container with the Rayleigh number $\mathrm{Ra} = 10^6$ and the Prandtl number $\mathrm{Pr} = 0.025$, compared with the data for the same conditions obtained earlier by direct numerical simulation (DNS).

The test computations indicate it was found that the grid size of about half a million cells is sufficient to predict time-averaged fields of velocity, temperature, local and integral heat transfer if we use a software tool implementing second-order numerical schemes. This conclusion can be extended to the case of problems on three-dimensional Rayleigh-Bénard convection of liquid metal with similar geometry. Grids whose number of cells is higher by an order of magnitude are necessary to accurately predict second-order statistics (total turbulent stresses and components of the turbulent heat flux vector),

All RANS models of turbulence used predict time-averaged velocity and temperature fields, as well as local heat transfer at the end walls, which are in good agreement with the DNS data. The integral values of the Nusselt number obtained for different RNS models differ from the DNS data by no more than 3.6%; a deviation towards lower values is observed for the *k*-ε RNG model, and towards higher values for the other two models. The Reynolds stress model gives the result closest to the one obtained by the DNS method.

The numerical solution obtained via the k-ω SST and RSM models on a grid of 3.7 million cells has a turbulent character, with a continuous spectrum of resolved fluctuations making a large contribution to statistical second-order characteristics. In contrast, the k-ε RNG model predicts unsteady convection flow with quasi-periodic fluctuations of low intensity, where the simulated component comprises nearly the entire contribution to second-order moments. The best agreement with the DNS data for total second-order moments was obtained by the Reynolds stress model.

In view of the above, the experience outlined in our paper for applying this approach to solving the model problem can be useful in numerical studies on a wide range of industrial and geophysical problems associated with Rayleigh–Bénard convection where a statistically significant or even decisive role is played by three-dimensional large-scale circulation.

REFERENCES

1. **Ahlers G., Grossmann S., Lohse D.,** Heat transfer and large scale dynamics in turbulent Rayleigh – Bénard convection, Rev. Mod. Phys. 81 (2) (2009) 503–538.

2. **Chilla F., Schumacher J.,** New perspectives in turbulent Rayleigh – Bénard convection, Eur. Phys. J. E. 35 (7) (2012) 58.

3. **Castaing B., Gunaratne G., Heslot F., et al.,** Scaling of hard thermal turbulence in Rayleigh – Bénard convection, J. Fluid Mech. 204 (July) (1989) 1–30.

4. **Ahlers G., Xu X.,** Prandtl-number dependence of heat transport in turbulent Rayleigh – Bénard convection, Phys. Rev. Lett. 86 (15) (2001) 3320–3323.

5. **Shishkina O., Thess A.,** Mean temperature profiles in turbulent Rayleigh –Bénard convection of water, J. Fluid Mech. 633 (25 August) (2009) 449–460.

6. **Li Y.-R., Ouyang Y.-Q., Peng L., Wu S.-Y.,** Direct numerical simulation of Rayleigh – Bénard convection in a cylindrical container of aspect ratio 1 for moderate Prandtl number fluid, Phys. Fluids. 24 (7) (2012) 074103.

7. **Lakkaraju R., Stevens R. J. A. M., Verzicco R., et al.,** Spatial distribution of heat flux and fluctuations in turbulent Rayleigh – Bénard convection, Phys. Rev. E. 86 (5) (2012) 056315.

8. **Cioni S., Ciliberto S., Sommeria J.,** Experimental study of high-Rayleigh-number convection in mercury and water, // Dyn. Atmos. Oceans. 24 (1) (1996) 117–127.

9. **Qui X.-L., Tong P.,** Large-scale velocity structures in turbulent thermal convection, Phys. Rev. E. 64 (3) (2001) 036304.

10. **Sreenivasan K. R., Bershadskii A., Niemela J. J.,** Mean wind and its reversal in thermal convection, Phys. Rev. E. 65 (5) (2002) 056306.

11. **Zürner T., Schindler F., Vogt T., et al.,** Combined measurement of velocity and temperature in liquid metal convection, J. Fluid Mech. 876 (10 October) (2019) 1108–1128.

12. **Abramov A. G., Ivanov N. G., Smirnov E. M.,** Numerical study of high-Ra Rayleigh – Bénard mercury and water convection in confined enclosures using a hybrid RANS/LES technique, Proc. Eurotherm Seminar 74 "Heat Transfer in Unsteady and Transitional Flows", March 23–26, 2003, Eindhoven, the Netherlands; Ed. by H. C. de Lange, A. A. van Steenhoven, TUE (2003) 33–38.

13. **Stevens R. J. A. M., Clercx H. J. H., Lohse D.,** Effect of plumes on measuring the large scale circulation in turbulent Rayleigh – Benard convection, Phys. Fluids. 23 (9) (2011) 095110.

14. **Mishra P. K., De A. K., Verma M. K., Eswaran V.,** Dynamics of reorientations and reversals of large-scale flow in Rayleigh – Bénard convection, J. Fluid Mech. 668 (10 February) (2011) 480–499.

15. **Schumacher J., Bandaru V., Pandey A., Scheel J. D.,** Transitional boundary layers in low-Prandtl-number convection, Phys. Rev. Fluids. 1 (8) (2016) 084402.

16. **Chilla F., Rastello M., Chaumat S., Castaing B.,** Long relaxation times and tilt sensitivity in Rayleigh – Bénard turbulence, Eur. Phys. J. B. 40 (2) (2004) 223–227.

17. **Brown E., Ahlers G.,** Rotations and cessations of the large-scale circulation in turbulent Rayleigh–Bénard convection, J. Fluid Mech. 568 (10 December) (2006) 351–386.

18. **Xi H.-D., Xia K.-Q.,** Azimuthal motion, reorientation, cessation, and reversal of the large-scale circulation in turbulent thermal convection: A comparative study in aspect ratio one and one-half geometries, Phys. Rev. E. 78 (3) (2008) 036326.

19. **Ji D., Bai K., Brown E.,** Effects of tilt on the orientation dynamics of the large-scale circulation in turbulent Rayleigh – Bénard convection, Phys. Fluids. 32 (7) (2020) 075118.

20. **Zwirner L., Khalilov R., Kolesnichenko I., et al.,** The influence of the cell inclination on the heat transport and large-scale circulation in liquid metal convection, J. Fluid Mech. 884 (10 February) (2020) A18.

21. **Shishkina O., Horn S.,** Thermal convection in inclined cylindrical containers // Journal of Fluid Mechanics. 790 (10 March) (2016) R3.

22. **Smirnov S. I., Abramov A. G., Smirnov E. M.,** Numerical simulation of turbulent Rayleigh – Bénard mercury convection in a circular cylinder with introducing small deviations from the axisymmetric formulation, J. Phys. Conf. Ser. 1359 (1) (2019) 012077.

23. **Smirnov S. I., Smirnov E. M.,** Direct numerical simulation of the turbulent Rayleigh – Bénard convection in a slightly tilted cylindrical contain, St. Petersburg State Polytechnical University Journal. Physics and Mathematics. 13 (1) (2020) 14–25 (in Russian).

24. **Smirnov S., Smirnovsky A., Bogdanov S.,** The emergence and identification of large-scale coherent structures in free convective flows of the Rayleigh – Bénard type, Fluids. 6 (12) (2021) 431–450.

25. **Van der Poel E. P., Stevens R. J. A. M., Lohse D.,** Comparison between two- and three-dimensional Rayleigh – Bénard convection, J. Fluid Mech. 736 (10 December) (2013) 177–194.

26. **Horn S., Shishkina O.,** Toroidal and poloidal energy in rotating Rayleigh – Bénard convection, J. Fluid Mech. 762 (10 January) (2015) 232–255.

27. **Scheel J. D., Schumacher J.,** Global and local statistics in turbulent convection at low Prandtl numbers, J. Fluid Mech. 802 (10 September) (2016) 147–173.

28. **Sakievich P. J., Peet Y. T., Adrian R. J.,** Large-scale thermal motions of turbulent Rayleigh–Bénard convection in a wide aspect-ratio cylindrical domain, Int. J. Heat Fluid Flow. 61 (2) (2016) 193–196.

29. **Kooij G. L., Botchev M. A., Frederix E. M. A., et al.,** Comparison of computational codes for direct numerical simulations of turbulent Rayleigh – Bénard convection, Comp. & Fluids. 166 (30 April) (2018) 1–8.

30. **Wan Z.-H., Wei P., Verzicco R., et al.,** Effect of sidewall on heat transfer and □ow structure in Rayleigh – Bénard convection, J. Fluid Mech. 881 (25 December) (2019) 218–243.

31. **Smirnov S. I., Smirnov E. M., Smirnovskiy A. A.,** Endwall heat transfer effects on the turbulent mercury convection in a rotating cylinder, St. Petersburg State Polytechnical University Journal. Physics and Mathematics. 10 (1) (2017) 31–46 (in Russian).

32. **Smirnov S. I., Smirnovskiy A. A.,** Numerical simulation of turbulent mercury natural convection in a heated-from-below cylinder with zero and non-zero thickness of the horizontal walls, Teplovyye Protsessy v Tekhnike [Thermal Processes in Technology]. 10 (3–4) (2018) 94–100 (in Russian).

33. **Borisov D. V., Kalaev V. V.,** ILES of melt turbulent convection with conjugated heat transfer in the crucible and gas flow for Czochralski silicon crystal growth system, J. Cryst. Growth. 573 (3) (2021) 126305.

34. **Kenjereš S., Hanjalić K.** Transient analysis of Rayleigh – Bénard convection with a RANS model, Int. J. Heat Fluid Flow. 20 (3) (1999) 329–340.

35. **Hanjalić K., Kenjereš S.,** Reorganization of turbulence structure in magnetic Rayleigh – Bénard convection: a T-RANS study, J. Turbul. 1 (8) (2000) 1–22.

36. **Kenjereš S., Hanjalić K.,** LES, T-RANS and hybrid simulations of thermal convection at high Ra numbers, Int. J. Heat Fluid Flow. 27 (5) (2006) 800–810.

37. **Choi S.-K., Han J.-W., Choi H.-K.,** Performance of second-moment differential stress and flux models for natural convection in an enclosure, Int. Commun. Heat Mass Transf. 99 (December) (2018) 54–61.

38. **Clifford C. E., Kimber M. L.,** Assessment of RANS and LES turbulence models for natural convection in a differentially heated square cavity, Numer. Heat Transf. Part A. 78 (10) (2020) 560–594.

39. **Levchenya A. M., Trunova S. N., Kolesnik E. V.,** Assessment of RANS turbulence models capabilities based on computational results for free convection developing near a suddenly heated vertical plate, St. Petersburg State Polytechnical University Journal. Physics and Mathematics. 13 (2) (2020) 27–40 (in Russian).

40. **Katsamis C., Craft T., Iacovides H., Uribe J. C.,** Use of 2-D and 3-D unsteady RANS in the computation of wall bounded buoyant flows, Int. J. Heat Fluid Flow. 93 (February) (2022) 108914.

41. **Levchenya A. M., Smirnov E. M., Trunova S. N.** Vliyaniye periodicheskoy makrosherokhovatosti na razvitiye turbulentnoy svobodnoy konvektsii u vnezapno nagrevayemoy vertikalnoy plastiny [The influence of periodical macroroughness on the development of free turbulent convection near a suddenly heated vertical plate], Pisma v Zhurnal Tekhnicheskoy Fiziki. 48 (3) (2022) 47–50 (in Russian).

42. **Orszag S. A., Yakhot V., Flannery W. S., et al.,** Renormalization group modeling and turbulence simulations, Proc. Int. Conf. Near-Wall Turbulent Flows, Tempe, Arizona, USA, 15–17 March (1993) 1031.

43. **Menter F. R.,** Two-equation eddy-viscosity turbulence models for engineering applications, AIAA J. 32 (8) (1994) 1598–1605.

44. **Menter F. R., Kuntz M., Langtry R.,** Ten 2022s of industrial experience with the SST turbulence model, In Book: Turbulence, Heat and Mass Transfer. Vol. 4. Proc. Fourth Int. Symp. Turbulence, Heat & Mass Transfer. Antalya, Turkey, 12–17 October (2003) 625–632.

45. **Launder B. E., Reece G. J., Rodi W.,** Progress in the development of a Reynolds-stress turbulence closure, J. Fluid Mech. 68 (3) (1975) 537–566.

46. **Gibson M. M., Launder B. E.,** Ground effects on pressure fluctuations in the atmospheric boundary layer, J. Fluid Mech. 86 (3) (1978) 491–511.

47. **Wilcox D. C.,** Turbulence modeling for CFD. 2nd edition, DCW Industries, La Canada, California, 1998.

СПИСОК ЛИТЕРАТУРЫ

1. **Ahlers G., Grossmann S., Lohse D.** Heat transfer and large scale dynamics in turbulent Rayleigh – Bénard convection // Reviews of Modern Physics. 2009. Vol. 81. No. 2. Pp. 503–538.

2. **Chilla F., Schumacher J.** New perspectives in turbulent Rayleigh – Bénard convection // The European Physical Journal. E. 2012. Vol. 35. No. 7. P. 58.

3. **Castaing B., Gunaratne G., Heslot F., Kadanoff L., Libchaber A., Thomae S., Wu X.-Z., Zaleski S., Zanetti G.** Scaling of hard thermal turbulence in Rayleigh – Bénard convection // Journal of Fluid Mechanics. 1989. Vol. 204. July. Pp. 1–30.

4. **Ahlers G., Xu X.** Prandtl-number dependence of heat transport in turbulent Rayleigh – Bénard convection // Physical Review Letters. 2001. Vol. 86. No. 15. Pp. 3320–3323.

5. **Shishkina O., Thess A.** Mean temperature profiles in turbulent Rayleigh –Bénard convection of water // Journal of Fluid Mechanics. 2009. Vol. 633. 25 August. Pp. 449–460.

6. **Li Y.-R., Ouyang Y.-Q., Peng L., Wu S.-Y.** Direct numerical simulation of Rayleigh – Bénard convection in a cylindrical container of aspect ratio 1 for moderate Prandtl number fluid // Physics of Fluids. 2012. Vol. 24. No. 7. P. 074103.

7. **Lakkaraju R., Stevens R. J. A. M., Verzicco R., Grossmann S., Prosperetti A., Sun C., Lohse D.** Spatial distribution of heat flux and fluctuations in turbulent Rayleigh – Bénard convection // Physical Review. E. 2012. Vol. 86. No. 5. P. 056315.

8. **Cioni S., Ciliberto S., Sommeria J.** Experimental study of high-Rayleigh-number convection in mercury and water // Dynamics of Atmospheres and Oceans. 1996. Vol. 24. No. 1. Pp. 117–127.

9. **Qui X.-L., Tong P.** Large-scale velocity structures in turbulent thermal convection // Physical Review. E. 2001. Vol. 64. No. 3. P. 036304.

10. **Sreenivasan K. R., Bershadskii A., Niemela J. J.** Mean wind and its reversal in thermal convection // Physical Review. E. 2002. Vol. 65. No. 5. P. 056306.

11. **Zürner T., Schindler F., Vogt T., Eckert S., Schumacher J.** Combined measurement of velocity and temperature in liquid metal convection // Journal of Fluid Mechanics. 2019. Vol. 876. 10 October. Pp. 1108–1128.

12. **Abramov A. G., Ivanov N. G., Smirnov E. M.** Numerical study of high-Ra Rayleigh – Bénard mercury and water convection in confined enclosures using a hybrid RANS/LES technique // Proceedings of the Eurotherm Seminar 74 “Heat Transfer in Unsteady and Transitional Flows”. March 23–26, 2003; Eindhoven, the Netherlands. Ed. by H. C. de Lange, A. A. van Steenhoven, TUE, 2003. Pp. 33–38.

13. **Stevens R. J. A. M., Clercx H. J. H., Lohse D.** Effect of plumes on measuring the large scale circulation in turbulent Rayleigh – Benard convection // Physics of Fluids. 2011. Vol. 23. No. 9. P. 095110.

14. **Mishra P. K., De A. K., Verma M. K., Eswaran V.** Dynamics of reorientations and reversals of large-scale flow in Rayleigh – Bénard convection // Journal of Fluid Mechanics. 2011. Vol. 668. 10 February. Pp. 480–499.

15. **Schumacher J., Bandaru V., Pandey A., Scheel J. D.** Transitional boundary layers in low-Prandtl-number convection // Physical Review Fluids. 2016. Vol. 1. No. 8. P. 084402.

16. **Chilla F., Rastello M., Chaumat S., Castaing B.** Long relaxation times and tilt sensitivity in Rayleigh – Bénard turbulence // The European Physical Journal. B. 2004. Vol. 40. No. 2. Pp. 223–227.

17. **Brown E., Ahlers G.** Rotations and cessations of the large-scale circulation in turbulent Rayleigh–Bénard convection // Journal of Fluid Mechanics. 2006. Vol. 568. 10 December. Pp. 351–386.

18. **Xi H.-D., Xia K.-Q.** Azimuthal motion, reorientation, cessation, and reversal of the large-scale circulation in turbulent thermal convection: A comparative study in aspect ratio one and one-half geometries // Physical Review. E. 2008. Vol. 78. No. 3. P. 036326.

19. **Ji D., Bai K., Brown E.** Effects of tilt on the orientation dynamics of the large-scale circulation in turbulent Rayleigh – Bénard convection // Physics of Fluids. 2020. Vol. 32. No. 7. P. 075118.

20. **Zwirner L., Khalilov R., Kolesnichenko I., Mamykin A., Mandrykin S., Pavlinov A., Shestakov A., Teimurazov A., Frick P., Shishkina O.** The influence of the cell inclination on the heat transport and large-scale circulation in liquid metal convection // Journal of Fluid Mechanics. 2020. Vol. 884. 10 February. P. A18.

21. **Shishkina O., Horn S.** Thermal convection in inclined cylindrical containers // Journal of Fluid Mechanics. 2016. Vol. 790. 10 March. P. R3.

22. **Smirnov S. I., Abramov A. G., Smirnov E. M.** Numerical simulation of turbulent Rayleigh – Bénard mercury convection in a circular cylinder with introducing small deviations from the axisymmetric formulation // Journal of Physics: Conference Series. 2019. Vol. 1359. No. 1. P. 012077.

23. Смирнов С. И., Смирнов Е. М. Прямое численное моделирование турбулентной конвекции Рэлея – Бенара в слегка наклоненном цилиндрическом контейнере // Научно-технические ведомости СПбГПУ. Физико-математические науки. 2020. Т. 13. № 1. С. 14–25.

24. **Smirnov S., Smirnovsky A., Bogdanov S.** The emergence and identification of large-scale coherent structures in free convective flows of the Rayleigh – Bénard type // Fluids. 2021. Vol. 6. No. 12. Pp. 431–450.

25. **Van der Poel E. P., Stevens R. J. A. M., Lohse D.** Comparison between two- and three-dimensional Rayleigh – Bénard convection // Journal of Fluid Mechanics. 2013. Vol. 736. 10 December. Pp. 177–194.

26. **Horn S., Shishkina O.** Toroidal and poloidal energy in rotating Rayleigh – Bénard convection // Journal of Fluid Mechanics. 2015. Vol. 762. 10 January. Pp. 232–255.

27. **Scheel J. D., Schumacher J.** Global and local statistics in turbulent convection at low Prandtl numbers // Journal of Fluid Mechanics. 2016. Vol. 802. 10 September. Pp. 147–173.

28. **Sakievich P. J., Peet Y. T., Adrian R. J.** Large-scale thermal motions of turbulent Rayleigh–Bénard convection in a wide aspect-ratio cylindrical domain // International Journal of Heat and Fluid Flow. 2016. Vol. 61. No. 2. Pp. 193–196.

29. **Kooij G. L., Botchev M. A., Frederix E. M. A., Geurts B. J., Horn S., Lohse D., van der Poel E. P., Shishkina O., Stevens R. J. A. M., Verzicco R.** Comparison of computational codes for direct numerical simulations of turbulent Rayleigh – Bénard convection // Computers & Fluids. 2018. Vol. 166. 30 April. Pp. 1–8.

30. **Wan Z.-H., Wei P., Verzicco R., Lohse D., Ahlers G., Stevens R. J. A. M.** Effect of sidewall on heat transfer and flow structure in Rayleigh – Bénard convection // Journal of Fluid Mechanics. 2019. Vol. 881. 25 December. Pp. 218–243.

31. **Смирнов С. И., Смирнов Е. М., Смирновский А. А.** Влияние теплопереноса в торцевых стенках на турбулентную конвекцию ртути во вращающемся цилиндре // Научно-технические ведомости СПбПУ. Физико-математические науки. 2017. Т. 10. № 1. С. 31–46.

32. **Смирнов С. И., Смирновский А. А.** Численное моделирование турбулентной свободной конвекции ртути в подогреваемом снизу цилиндре при нулевой и конечной толщине горизонтальных стенок // Тепловые процессы в технике. 2018. Т. 10. № 3–4. С. 94–100.

33. **Borisov D. V., Kalaev V. V.** ILES of melt turbulent convection with conjugated heat transfer in the crucible and gas flow for Czochralski silicon crystal growth system // Journal of Crystal Growth. 2021. Vol. 573. No. 3. P. 126305.

34. **Kenjereš S., Hanjalić K.** Transient analysis of Rayleigh – Bénard convection with a RANS model // International Journal of Heat and Fluid Flow. 1999. Vol. 20. No. 3. Pp. 329–340.

35. **Hanjalić K., Kenjereš S.** Reorganization of turbulence structure in magnetic Rayleigh – Bénard convection: a T-RANS study // Journal of Turbulence. 2000. Vol. 1. No. 8. Pp. 1–22.

36. **Kenjereš S., Hanjalić K.** LES, T-RANS and hybrid simulations of thermal convection at high Ra numbers // International Journal of Heat and Fluid Flow. 2006. Vol. 27. No. 5. Pp. 800–810.

37. **Choi S.-K., Han J.-W., Choi H.-K.** Performance of second-moment differential stress and flux models for natural convection in an enclosure // International Communications in Heat and Mass Transfer. 2018. Vol. 99. December. Pp. 54–61.

38. **Clifford C. E., Kimber M. L.** Assessment of RANS and LES turbulence models for natural convection in a differentially heated square cavity // Numerical Heat Transfer. Part A. 2020. Vol. 78. No. 10. Pp. 560–594.

39. Левченя **А. М.,** Трунова **С. Н., Колесник Е. В.** Оценка возможностей RANS-моделей турбулентности по результатам расчетов свободной конвекции, развивающейся вблизи внезапно нагретой вертикальной пластины // Научно-технические ведомости СПбГПУ. Физико-математические науки. 2020. Т. 13. № 2. С. 27–40.

40. **Katsamis C., Craft T., Iacovides H., Uribe J. C.** Use of 2-D and 3-D unsteady RANS in the computation of wall bounded buoyant flows // International Journal of Heat and Fluid Flow. 2022. Vol. 93. February. P. 108914.

41. **Левченя А. М., Смирнов Е. М.,** Трунова **С. Н.** Влияние периодической макрошероховатости на развитие турбулентной свободной конвекции у внезапно нагреваемой вертикальной пластины // Письма в Журнал технической физики. 2022. Т. 48. № 3. С. 47–50.

42. **Orszag S. A., Yakhot V., Flannery W. S., Boysan F., Choudhury D., Maruzewski J., Patel B.** Renormalization group modeling and turbulence simulations // Proceedings of the International Conference on Near-Wall Turbulent Flows, Tempe, Arizona, USA, 15–17 March 1993. P. 1031.

43. **Menter F. R.** Two-equation eddy-viscosity turbulence models for engineering applications // AIAA Journal (Journal of the American Institute of Aeronautics and Astronautics). 1994. Vol. 32. No. 8. Pp. 1598–1605.

44. **Menter F. R., Kuntz M., Langtry R.** Ten 2022s of industrial experience with the SST turbulence model // Turbulence, Heat and Mass Transfer. Vol. 4. Proceedings of the Fourth International Symposium on Turbulence, Heat and Mass Transfer. Antalya, Turkey, 12–17 October, 2003. Pp. 625–632.

45. **Launder B. E., Reece G. J., Rodi W.** Progress in the development of a Reynolds-stress turbulence closure // Journal of Fluid Mechanics. 1975. Vol. 68. No. 3. Pp. 537–566.

46. **Gibson M. M., Launder B. E.** Ground effects on pressure fluctuations in the atmospheric boundary layer // Journal of Fluid Mechanics. 1978. Vol. 86. No. 3. Pp. 491–511.

47. **Wilcox D. C.** Turbulence modeling for CFD. 2nd edition. La Canada, California: DCW Industries, 1998. 457 p.

THE AUTHORS

SMIRNOV Sergei I.
Peter the Great St. Petersburg Polytechnic University
29 Politechnicheskaya St., St. Petersburg, 195251, Russia
sergeysmirnov92@mail.ru
ORCID: 0000-0002-3972-9259

SMIRNOV Evgeny M.
Peter the Great St. Petersburg Polytechnic University
29 Politechnicheskaya St., St. Petersburg, 195251, Russia
smirnov_em@spbstu.ru
ORCID: 0000-0002-7218-6372

СВЕДЕНИЯ ОБ АВТОРАХ

СМИРНОВ Сергей Игоревич – *кандидат физико-математических наук, инженер научно-образовательного центра «Компьютерные технологии в аэродинамике и теплотехнике» Санкт-Петербургского политехнического университета Петра Великого.*
195251, Россия, г. Санкт-Петербург, Политехническая ул., 29
sergeysmirnov92@mail.ru
ORCID: 0000-0002-3972-9259

СМИРНОВ Евгений Михайлович – *доктор физико-математических наук, профессор Высшей школы прикладной математики и вычислительной физики Санкт-Петербургского политехнического университета Петра Великого.*
195251, Россия, г. Санкт-Петербург, Политехническая ул., 29
smirnov_em@spbstu.ru
ORCID: 0000-0002-7218-6372

Received 01.04.2022. Approved after reviewing 06.06.2022. Accepted 06.06.2022.
Статья поступила в редакцию 01.04.2022. Одобрена после рецензирования 06.06.2022. Принята 06.06.2022.